J Mol Model (2011) 17:505–514
DOI 10.1007/s00894-010-0741-5

ORIGINAL PAPER

# The adsorption of mercury-species on relaxed and rumpled CaO (0 0 1) surfaces investigated by density functional theory

**Paul Blowers · Bo Gyeong Kim**

Received: 26 August 2009 / Accepted: 3 May 2010 / Published online: 28 May 2010


**Abstract** This research examines the importance of several computational choices in modeling mercury species adsorption on calcium oxide surfaces and is the second in a series of papers. The importance of surface relaxation was tested and it was found that adsorption energies changed for $HgCl_2$, moving adsorption from being at the borderline of physisorption and chemisorption to being strongly chemisorbed. Results for Hg and HgCl were unaffected. A second computational choice, that of the cluster or periodic model size was tested in both the plane of the model (4×4 or 5×5 model sizes) and for the depth (two or three layers). It was found that the minimum cluster size for handling mercury adsorption was 5×5 and that only two layers of depth were needed. The energetic results show that rumpled CaO surfaces will only weakly physisorb elemental mercury, but could be used to capture $HgCl_2$ from coal combustion flue gases, which is in agreement with limited experimental data.

**Keywords** Adsorption energy · DFT · Equilibrium constants · Mercury · Surface relaxation

## Introduction

Mercury is a ubiquitous chemical element in the environment and is a unique metal which has a high vapor pressure and exists as a liquid at ambient conditions. It has high volatility and is easily transported between environmental compartments where it is distributed on a global scale. There are two types of global mercury emission sources, natural and anthropogenic. Natural sources contribute 70 percent of the global mercury emissions and anthropogenic sources account for the rest of the total mercury released to the environment [1]. The amount of mercury emissions from man-made sources has been increasing during the last few decades, mainly due to fossil fuel combustion which has distributed 810 Mg $yr^{-1}$ to global mercury emissions. This amount accounts for the second largest emission source of total mercury emissions, and is the major anthropogenic source. Industrial point sources could be controlled by mercury removal technologies to reduce the large anthropogenic mercury emissions. This research focuses specifically on mercury removal from the flue gases of coal-fired power plants.

There are few commercially available flue gas treatment technologies, but generally coal-fired power plants use wet scrubbing or activated carbon injection methods [2–13]. Elemental mercury is difficult to control because of its insolubility in water. However, wet scrubbers can achieve 70–85% mercury removal with an oxidizing agent that converts elemental mercury to oxidized mercury, $HgCl_2$. If HCl or $Cl_2$, or other oxidizing agents are not injected into the flue gases, then total mercury removal is no greater than 50 percent [14, 15]. Sulfur dioxide ($SO_2$) in the flue gas plays a counteracting reducing function that transforms oxidized mercury to elemental mercury, which allows subsequent pollution to the environment.

The most prominent mercury control system is activated carbon injection (ACI) which achieves mercury reduction at least 85 percent [15]. The injection of activated carbon in the stack exhaust gas has been used successfully when it is placed before a particulate collection device. This promising system allows elemental mercury to be removed from

P. Blowers (✉) · B. G. Kim
Department of Chemical and Environmental Engineering,
The University of Arizona,
Tucson, AZ 85721-0011, USA
e-mail: blowers@engr.arizona.edu

the flue gas. The most important factors in the efficacy of activated carbon in capturing mercury from the flue gas include the flue gas temperature, mercury concentration, chloride content and the volumetric flow rate of the flue gas. If even one of these operating parameters is out of a narrow range of acceptability, then performance of this mercury control system is largely ineffective. Activated carbon injection thus, has limitations for its application because removal effectiveness depends on the expensive operating conditions. For instance, these systems must operate at low temperatures, and the cooling costs for the stack gases are high, leading to a cost effectiveness that is in the range of $67,700–$70,000 per pound of mercury removed. Additionally, carbon-based sorbents deteriorate the quality of the fly ash after mercury removal, limiting the use of fly ash in building materials, in addition to having leaching problems at high temperatures where mercury species desorb from the surface [16].

The current challenge is to find sorbents that are effective at high temperatures while also being inexpensive. Paper Waste Derived Sorbent (PWDS), in market under the name MinPlus, is newly-developed and has proved to be effective at high temperatures in a bench scale Hg control system [17]. Mercury adsorption on this sorbent appears to be irreversible, and there is a possibility of using the highly stable MinPlus-Hg product in construction materials if leaching or mercury re-emission can be prevented. MinPlus is also a waste product from paper recycling producers, indicating it could be a green design solution to mercury emissions control.

The energetics and mechanisms of mercury adsorption on the MinPlus sorbent are not well understood. In the flue gases, mercury exists in the elemental form [18] but some of it is oxidized into Hg(I) and Hg(II) forms as HgCl and HgCl2 promoted by the presence of chlorine, as proposed by Sliger et al. [19, 20]. The unstable gas form of HgCl is directly oxidized to HgCl2 in flue gases. Calcium oxide (CaO) is one of the main components of MinPlus which has a composition that is 23% CaO, 29% Al2O3·SiO2, 41% CaCO3, 6% inert and 1% Ca(OH)2. Based on differential thermal analysis of the MinPlus sorbent, the CaCO3 is converted through calcination into CaO and CO2, as is Ca(OH)2, leading to CaO making up more than 50% of the MinPlus sorbent at elevated temperatures. In this research, we used the CaO structure which is the resulting predominant constituent of the MinPlus sorbent. In this study, the adsorption of mercury-species (Hg, HgCl and HgCl2) on the CaO (0 0 1) surface was investigated using density functional theory calculations. This investigation on relaxed CaO surfaces is part of a series on adsorption of mercury-containing species on MinPlus sorbents.

In previous work, we investigated the adsorption of mercury-species on fixed CaO surfaces [21]. However, relaxation effects play an important role in predicting adsorption energies of species on oxidized metal surfaces [22]. For instance, recent work looked at adsorption of $NO_x$ and other species on a relatively small CaO cluster that was allowed to relax during geometry optimization at the B3LYP level [23]. The authors found that relaxation enhances stabilities and increases binding energies.

To investigate Hg, HgCl and $HgCl_2$ adsorption, we considered clean non-defective CaO surface models while accounting for surface relaxation. The surface calculations employed cluster models that have proved to be successful for simulating metal oxide surfaces [24–27], but periodic slab calculations were also done. We confirm again in this work that the 5×5 unit cell of the CaO surface is the critical cluster size to obtain reliable adsorption energies for mercury-containing species while avoiding edge effects. In order to investigate the influence of surface layers on surface relaxation, we tested mercuric chloride adsorption on both CaO 5×5×2 and 5×5×3 surface structures. The $HgCl_2$ adsorption model for the relaxed CaO surfaces placed adsorption in the chemisorption range while the $HgCl_2$ adsorption model on the fixed CaO surface is at the border between physisorption and chemisorption. Since relaxation plays a significant role in this adsorption system, we chose to investigate the effect of the number of surface layers on energetics of $HgCl_2$ adsorption after surface relaxation.

The geometry optimization results, relaxation effects and adsorption energies of the Hg-species adsorption models are discussed in Sects. 1 and 2. Then temperature effects on equilibrium constants are described in Sect. 3 since the equilibrium constants are strongly dependent on temperature. HOMO and LUMO energy analysis of mercury-containing species on 5×5×2 CaO clusters were done to probe the stabilities of the adsorption models and are discussed in Sect. 4. Finally, the adsorption results for relaxed CaO surfaces are compared with adsorption energies for mercury-species on the flat fixed CaO surfaces explored in previous work.

## Methods

The theoretical calculations based on density functional theory (DFT) were performed using the $DMol^3$ package [28] in the Accelrys Materials Studio 2001 [29]. The local density approximation (LDA) was combined with the PWC functional [30], which optimizes geometries reliably [31]. The LDA method calculates less accurate energetics, even if it leads to accurate geometry optimization [32–37]. Therefore, the generalized gradient approximation (GGA) was combined with the BLYP correlation functional [37–40] for more accurate single point energy calculations using the geometries

optimized at the LDA level to give improved energetics. We tested DND and DNP basis sets on the $HgCl_2$ molecule to determine which basis set leads to more reliable results. When the entropy values at standard state were compared with experimental data from the NIST webbook, the DND basis set showed higher accuracy [41]. The entropy of $HgCl_2$ reported in the NIST webbook is 294.78 $Jmol^{-1}K^{-1}$ at the standard state. The percent error of the theoretically calculated entropy with the DND basis set was 8.8% compared to the reference entropy, while the error with the DNP basis set was 9.5%. Therefore, we used the DND basis set and the all electron method for all cluster and periodic slab models in this work.

A clean 5×5×2 cluster model and 5×5×2 and 5×5×3 periodic slabs with no defects were employed. These cluster models have low Hg coverage at 4.0% to approximate adsorption on clean adsorbents. The Hg coverage for the periodic slab is also 4.0% since the surface was designed with a 5×5 unit cell. A two layered surface was employed to investigate interactions between the adsorbate and surface which has proven to be accurate in the past [42–44]. However, we also employed both two and three layered surfaces for the CaO surface in order to compare relaxation due to the number of layers. Adsorption processes of $HgCl_2$ on 5×5×2 and 5×5×3 periodic slabs were investigated because this species had the strongest relaxation effect. The top layer was allowed to relax during the geometry optimization. All CaO (0 0 1) structures were started with bond lengths of 2.405 Å for the two layered model and 2.304 Å for the three layered structure, which is the default for the CaO (0 0 1) cleaved surface in $DMol^3$. The periodic slab geometries were infinitely extended to avoid edge effects and to reduce computational time. The periodic system studied used a vacuum thickness of 10 Å that was chosen to eliminate spurious interactions between the adsorbate and the periodic image of the bottom layer of the surface which would appear on top of the 5×5 unit cell. Also, the calculations were performed with 4×4×1 mesh k-points by the Monkhorst-Pack scheme for the 5×5×2 CaO model and 5×5×2 k-point set for the 5×5×3 CaO system.

Results were obtained with spin unrestricted polarization calculations. The spin unpolarized calculations were conducted for adsorbed elemental mercury and each clean cluster, while spin polarized calculations were conducted for adsorbed oxidized mercury species for the cluster models and periodic slabs because spin polarization could have an effect on the adsorption energies. However, when we investigated spin-restricted and-unrestricted calculations for Hg on a 4×4×2 surface in the previous work, the adsorption energy difference was ~2.1 kJ $mol^{-1}$, which is too small to impact results. Spin-orbit coupling effects are neglected in the scalar relativistic approach based on prior research with other mercury calculations [45–47]. BSSE (basis set superposition error) contributions have not been accounted for because, technically, the BSSE calculations are unavailable in $DMol^3$. However, the numerical basis functions of $DMol^3$ are more complete functions than Gaussian functions and are expected to have small BSSE contributions while *ab initio* methods use BSSE calculations to estimate the errors associated with their incomplete basis sets [48].

## Results and discussion

### Optimized geometries

Most mercury molecules moved to, and adsorbed atop, the middle oxygen atom of the surface after geometry optimization when many different starting configurations for the mercury-containing species were used on the CaO surfaces. The geometries presented in Fig. 1 are the most stable ones and we investigated geometries and energetics using the most stable configurations in this research. The fully optimized geometries for Hg, HgCl and $HgCl_2$ adsorption models on the relaxed CaO 5×5×2 cluster, 5×5×2 and 5×5×3 periodic slabs using the LDA/PWC method are represented in Fig. 1. The mercury adsorbates were initially placed horizontally on the surface with mercury oriented towards the oxygen site and the chlorine towards the calcium site. The mercury adsorbed on an atop site of the middle oxygen while chlorine bonded with the calcium sites on the 5×5×2 cluster and periodic slabs after optimization. The bond lengths are listed in Table 1. It should be noted that, when we tested the adsorption on the 4×4×2 cluster for evaluating the reliability of cluster size, the mercury-containing species on the that cluster adsorbed quite differently from the other models. The mercury species were shifted on the 4×4×2 surfaces with mercury moved from the atop site of oxygen toward a hollow site. The bond lengths of the Hg – O bond on the 4×4×2 cluster became longer as the mercury was oxidized; the distance between mercury for Hg, HgCl and $HgCl_2$ and oxygen on the surface were 3.352, 3.772, and 4.147 Å. While the 4×4×2 model led to longer bond distances, the energies indicated stronger adsorption energies than on the 5×5×2 cluster and periodic slab models. The edge oxygen atoms were noticeably contracted and this strongly influenced the bond lengths and adsorption energies, showing that this cluster is not large enough to model this system. Therefore, the unreliable results of the 4×4×2 cluster are not reported in this paper.

The distances between mercury for Hg, HgCl and $HgCl_2$ and oxygen on the 5×5×2 cluster were 3.34 Å, 2.51 Å and

2.28 Å, respectively. Mercury has a shorter distance to oxygen as mercury is oxidized on the 5×5×2 and periodic models. The chlorine atom contributes to the shorter Hg – O bond although Cl bonds further from the surface calcium; the bond lengths between Cl and Ca were 2.86 Å for HgCl and 3.02±0.05 Å for $HgCl_2$ on the 5×5×2 cluster surface. The optimized geometries of mercury-species on the periodic slabs have the same trends as the 5×5×2 cluster model. Interestingly, when the Hg-species were adsorbed on the relaxed 5×5×2 surface, the structural configurations of the adsorbates after optimization were different from adsorption on the fixed surfaces [21]. The mercury on the relaxed CaO surface moved closer to the surface as chlorine atoms moved farther away from the calcium atoms of the surface. However, the $HgCl_2$ molecule on the fixed CaO surface had the opposite trends.

The adsorption of mercury-species containing chlorine on the 5×5×2 cluster and periodic slabs led to positive $\Delta d$(Å) relaxation values. The relaxation results are reported in Table 1, where the distance change between two consecutive layers after optimization, the initial default distance and percentages of the surface relaxation are shown. The distance change is defined as $\Delta d = \{[z(Ca-O)_i] - [z(Ca-O)_j]\}/[z(Ca-O)_j]$. Indices $i$ indicated the distance between the first relaxed layer and the bottom layer, and $j$ indicates the initial default distance in the 5×5×2 periodic system. Indices $i$ and $j$ for the 5×5×3 periodic slab are represented in Fig. 2. The percentages of the surface relaxation for Hg, HgCl and

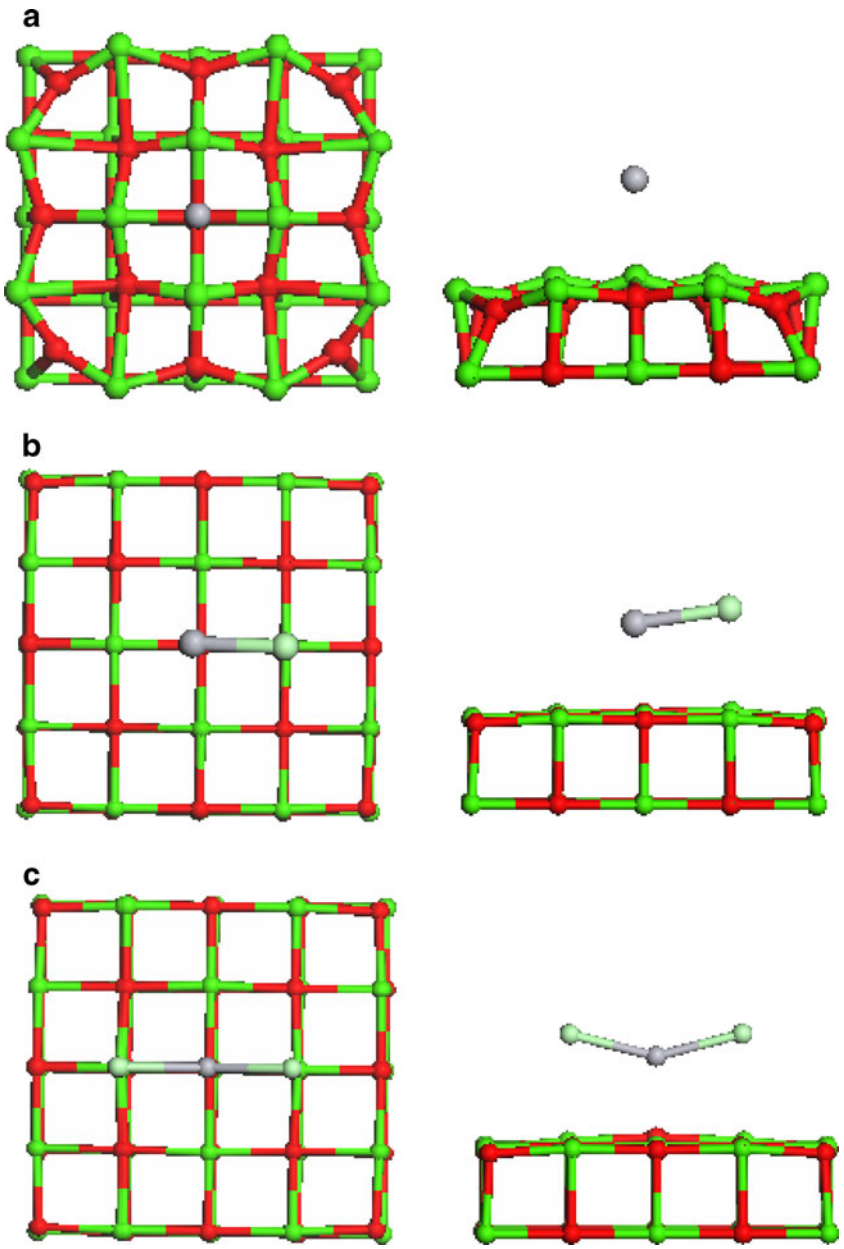


**Fig. 1** The top views and side views of optimized geometries for Hg, HgCl and $HgCl_2$ adsorption models on the relaxed CaO 5×5×2 cluster and periodic slab (red atom: oxygen, green atom: calcium and gray atom: mercury)

**Fig. 1** (continued)

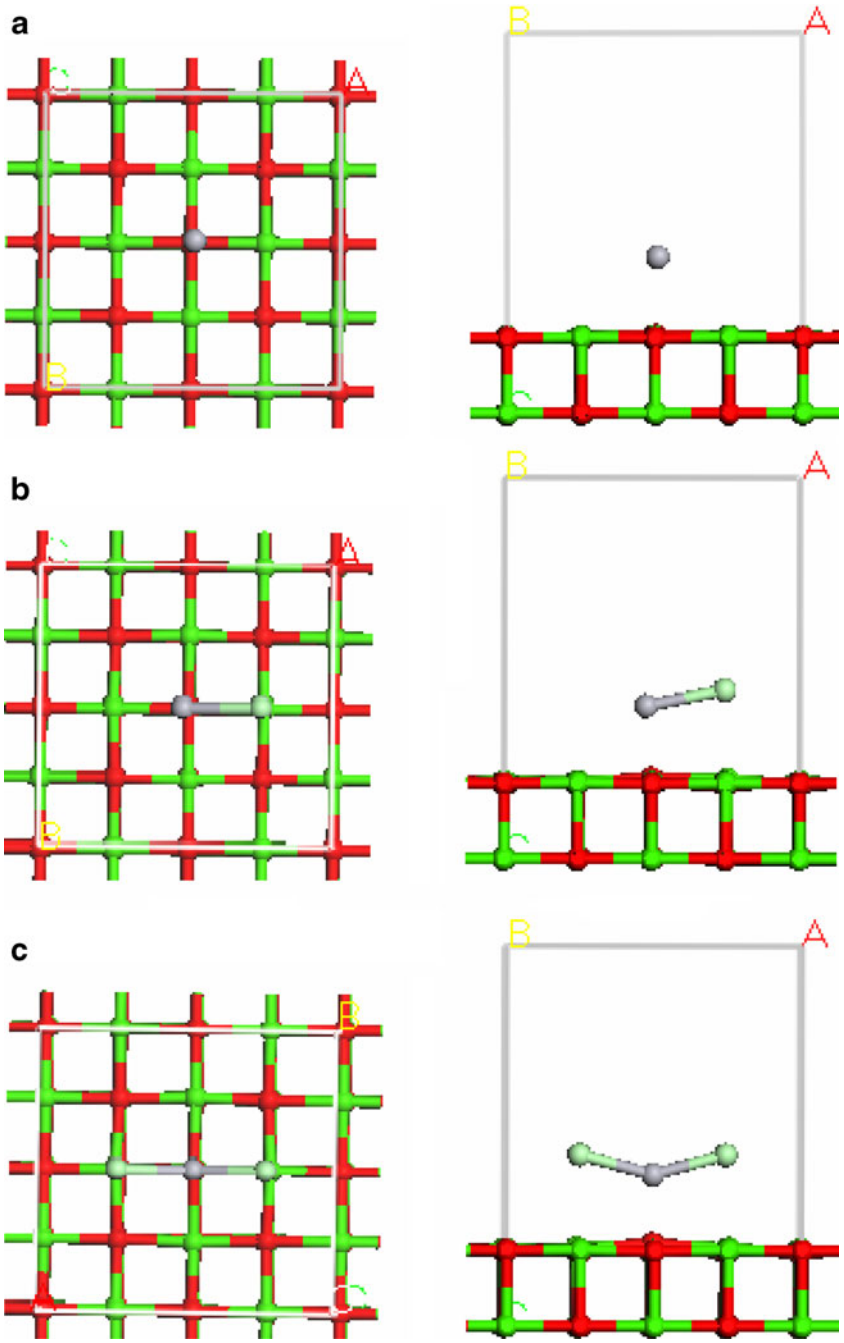


$HgCl_2$ adsorption on the 5×5×2 clusters were -10.69, 5.24 and 10.56%, respectively. The percentages of Δd(Å) relaxation values after $HgCl_2$ adsorption on the 5×5×2 and 5×5×3 periodic slabs were 11.6% and 15.32%, respectively. The $HgCl_2$ adsorption on the 5×5×2 periodic slab has only a % difference from the 5×5×3 periodic model. This suggests that the number of surface layers has no significant effect on the geometry of the relaxation process for mercury species adsorption on the CaO periodic surface. This result is consistent with the result that two surface layers of metal-oxide are enough to investigate interactions between these adsorbates and the adsorbent surfaces.

## Adsorption energies

The adsorption energies were calculated with the GGA/BLYP method using optimized structures obtained from the LDA/PWC calculations where the energies are defined by

$$\Delta E_{ads} = E_{Hg-species,surface} - \left(E_{Hg-species} + E_{surface}\right) \quad (1)$$

**Fig. 1** (continued)

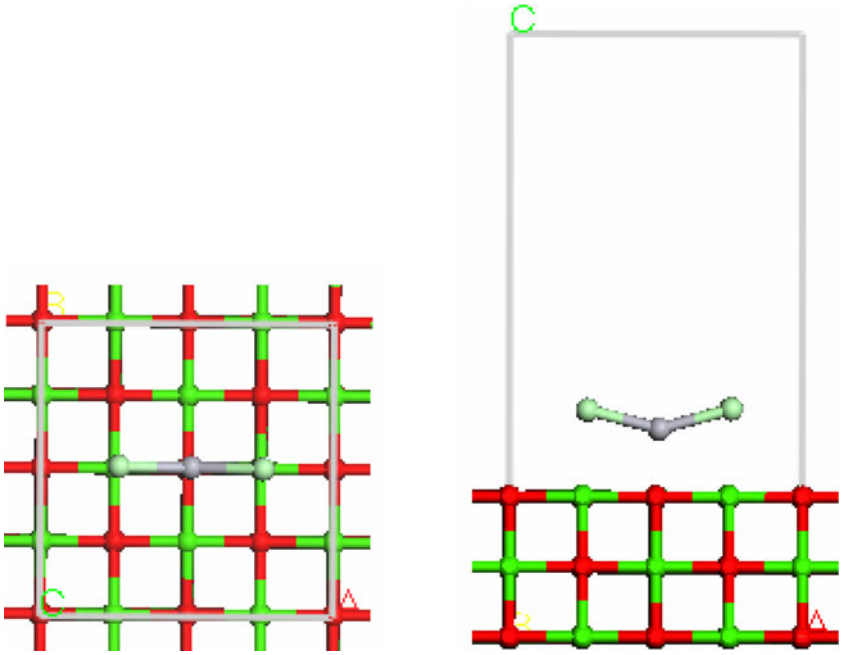

The adsorption energies are listed in Table 1. The GGA/BLYP adsorption energies of elemental mercury on the 5×5×2 cluster, and the periodic structure were -27.11, and -23.01 kJ mol$^{-1}$, respectively, which places them in the physical adsorption range [49]. The modeled CaO structures are unfavorable for elemental mercury adsorption, even when the relaxation effect is included. However, the adsorption energies for $HgCl_2$ on the 5×5×2 cluster and the periodic structure are -149.33 and -147.57 kJ mol$^{-1}$, respectively, and indicate chemisorption. The oxidized mercury formed with chlorine in the flue gases [19, 20] favorably enhances the adsorption ability of mercury on the relaxed CaO surface. Also, the adsorption energy of $HgCl_2$ on the three layered periodic system is -119.49 kJ mol$^{-1}$, also in the chemisorption range. They are different by ~28 kJ mol$^{-1}$, which not attribute to the chemisorption range. It indicates that the number of surface layers has no significant effect on adsorption energies;

There were no large differences in adsorption energies for elemental mercury and HgCl on fixed and relaxed calcium oxide surfaces which had ~4.184 kJ mol$^{-1}$ energy differences. The HgCl molecule has an unpaired electron and this leads to stronger interactions with the modeled fixed CaO surfaces. In general, the effect of relaxation was small when adsorption was clearly in either the physisorption or chemisorption ranges according to the adsorption energies of Hg and HgCl. On the other hand, relaxation plays an important role moving some mercury species over the threshold between physisorption and chemisorption. For instance, the adsorption energy of $HgCl_2$ on the 5×5×2 rumpled cluster and the periodic slab are -149.33 and -147.57 kJ mol$^{-1}$, respectively, but are -78.37 and -49.92 kJ mol$^{-1}$ on the corollary fixed surfaces. The relaxation effect moved the weak adsorption energy for the fixed surface to stronger adsorption for the relaxed surface.

## Temperature effect on equilibrium constants

In order to calculate thermodynamic data, we used general relationships for statistical thermodynamic partition functions (translational, rotational, and vibrational partition functions). Contributions from electronic motion are neglected due to the electronic ground state of our adsorption systems. The equilibrium constant was calculated by

$$\ln(K_{eq}) = \frac{-\Delta G}{RT}, \tag{2}$$

where $\Delta G$is the Gibbs free energy change, R is the ideal gas constant, and T is the temperature. The change of the Gibbs free energy during the adsorption process, $\Delta G$is defined as

$$\Delta G \approx \Delta E_{ads} + \Delta E_0 + T\left(\Delta S_{vib} + \Delta S_{trans,rot}\right) - kT\ln\left(\frac{P}{P_0}\right). \tag{3}$$

The change of adsorption energy ($\Delta E_{ads}$), change in zero-point energy ($\Delta E_o$)and entropy changes for the adsorption process were found through the atomistic calculation method developed by Loffreda [50]. The pressure terms cancel out because the mercury adsorption for these simulations assumes constant pressure due to low coverage. The equilibrium constants and Gibbs free energy were calculated as functions of temperature and were investigated in the

**Table 1** The bond distances between mercury adsorbates on the surfaces calculated at the LDA/PWC level, adsorption energies with GGA/BLYP, the surface relaxation (Δd) and percentage calculated with respect to the default distance (2.405 Å and 2.304 Å) on 5×5×2 and 5×5×3 surfaces from DMol are listed, respectively. To compare the results, the adsorption energies on fixed CaO surfaces are also listed below

| | CaO(5×5×2) | | | CaO(5×5×2 Periodic) | | | CaO(5×5×3 Periodic) |
|---|---|---|---|---|---|---|---|
| | Hg | HgCl | $HgCl_2$ | Hg | HgCl | $HgCl_2$ | $HgCl_2$ |
| LDA/PWC | | | | | | | |
| R(Hg-O) (Å) | 3.34 | 2.51 | 2.28 | 2.58 | 2.39 | 2.26 | 2.27 |
| R(Cl1-Hg) (Å) | | 2.65 | 2.50 | | 2.60 | 2.48 | 2.47 |
| R(Cl2-Hg) (Å) | | | 2.50 | | | 2.48 | 2.46 |
| R(Cl1-Ca) (Å) | | 2.86 | 3.02 | | 2.91 | 3.06 | 3.02 |
| R(Cl2-Ca) (Å) | | | 3.03 | | | 3.06 | 3.03 |
| GGA/BLYP | | | | | | | |
| $E_{ads}$(kJ/mol) | -27.11 | -160.46 | -149.33 | -23.01 | -165.18 | -147.57 | -119.49 |
| $E_{ads}$(kJ/mol)[a] | -26.48 | -154.81 | -78.37 | -27.32 | -129.49 | -49.92 | |
| Relaxation effect | | | | | | | |
| Δd(Å) | -0.26 | 0.13 | 0.25 | 0.13 | 0.19 | 0.27 | 0.35 |
| Relaxation % | -10.69 | 5.24 | 10.56 | 5.24 | 8.02 | 11.23 | 15.32 |

$E_{ads}$(kcal $mol^{-1}$)[a] : adsorption energies on fixed CaO surfaces [18]

temperature range of 250–1400 K because experiments indicate this range is appropriate.

Figures 3, 4, and 5 show that the equilibrium constants for all mercury-species on the 5×5×2 clusters, two layered periodic slab and three layered periodic slab increase as temperature decreases. The figures are consistent with these being exothermic systems [7]. The calculated entropy, Gibbs free energy changes, and equilibrium constants of $HgCl_2$ adsorption on the relaxed CaO 5×5×2 and 5×5×3 periodic slabs are shown in Table 2. Even though $HgCl_2$ adsorption on the relaxed CaO 5×5×2 periodic slab has higher entropies than the CaO 5×5×3 periodic slab, the trends of equilibrium constants are the same. As temperatures approach around 500 K, the equilibrium constant values on the 5×5×2 CaO surface are identical to the 5×5×3 CaO slab model results. Representation of equilibrium constants of $HgCl_2$ on 5×5×2 and 5×5×3 periodic slabs *vs*. temperature effects shown in Fig. 5 indicate both adsorption systems have a similar slope at all temperatures. However, $HgCl_2$ adsorption on the 5×5×2 periodic model has a gradually larger slope as temperatures go below 450 K. At extremely low or high temperatures, the number of surface layers influences thermodynamic properties of mercury adsorption systems because of the vibrational entropy dependency on the temperature. When the results of $HgCl_2$ adsorption on the relaxed surface were compared with the equilibrium constants on fixed surfaces, the relaxation effect contributed to more favorable adsorption at all temperatures. The ability to adsorb $HgCl_2$ on the periodic slab approaches the same values for equilibrium adsorbability of HgCl at high temperatures. The high adsorbability of $HgCl_2$ is important for real flue gas systems because, for oxidized mercury, the mercury predominantly exists as $HgCl_2$ and not HgCl. The employed CaO surfaces are more effective at capturing the oxidized mercury rather than elemental mercury at all temperatures.

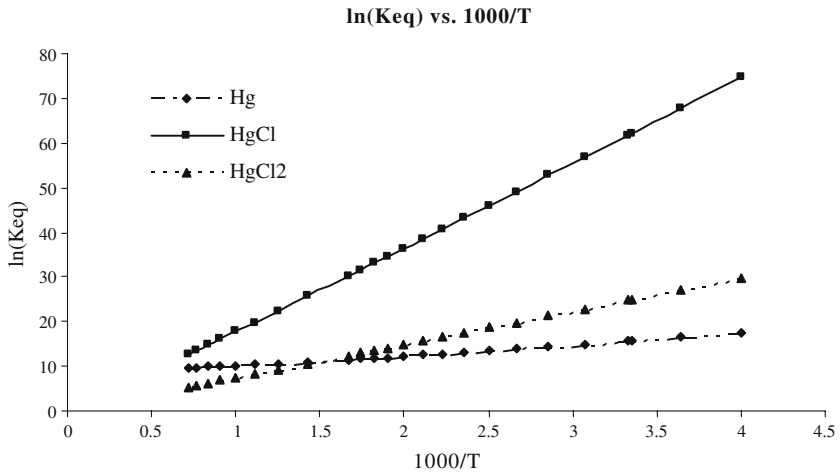


**Fig. 2** Representation of equilibrium constants of Hg, HgCl and $HgCl_2$ on 5×5×2 cluster *vs*. temperature effects. The adsorptions of the oxidized mercury species are favorable at low temperature

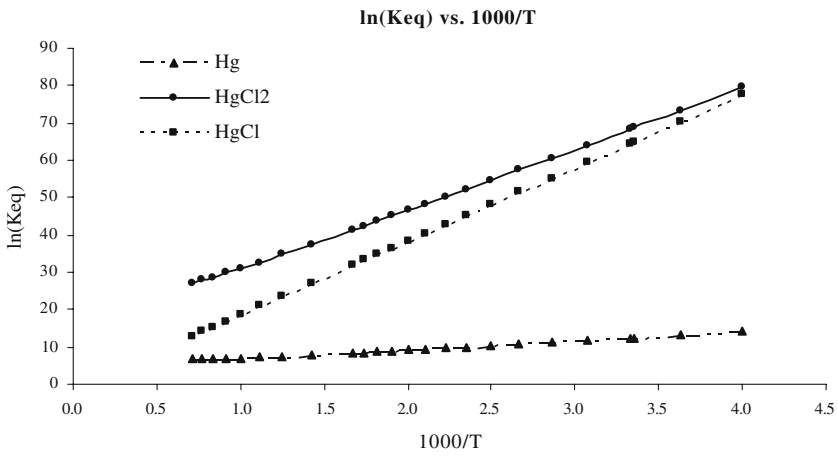


**Fig. 3** Representation of equilibrium constants of Hg, HgCl and $HgCl_2$ on 5×5×2 periodic slab *vs*. temperature effects. The adsorptions of the oxidized mercury species are favorable at low temperature

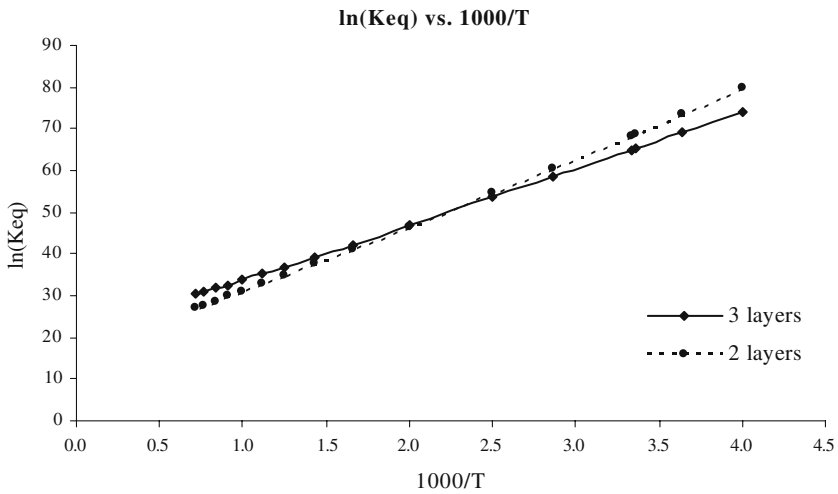


**Fig. 4** Representation of equilibrium constants of $HgCl_2$ on 5×5×2 and 5×5×3 periodic slabs *vs*. temperature effects

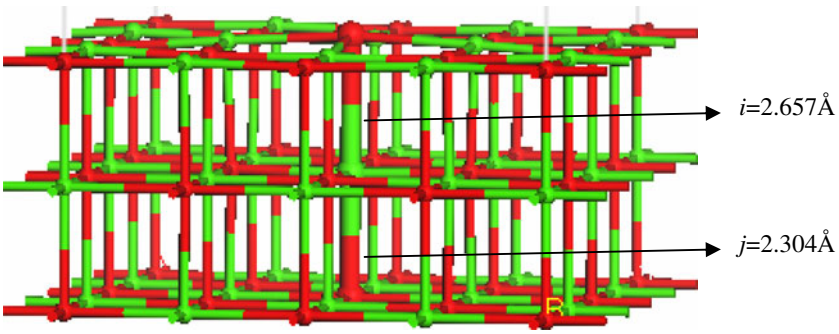


**Fig. 5** Representation of indices *i* and *j* on 5×5×3 periodic slab. Indices *i* indicated the distance between the first relaxed layer and the second layer, and *j* indicated the fixed default distance in 5×5×3 periodic system

**Table 2** The results of equilibrium constants, ΔS (J $mol^{-1}$ $K^{-1}$) and ΔG (kJ $mol^{-1}$) for $HgCl_2$ adsorptions on the relaxed CaO 5×5×2 and 5×5×3 periodic slabs within 250 K ~1400 K ($ln(K_{eq})$, ΔS and ΔG *vs*. 1000/T)

| T(K) | 1000/T | ln(Keq) | | ΔG (kJ/mol) | | ΔS (J/molK) | |
|---|---|---|---|---|---|---|---|
| | | 3 layers | 2 layers | 3 layers | 2 layers | 3 layers | 2 layers |
| 250 | 4.00 | 74.08 | 79.61 | -165.46 | -162.92 | -144.19 | -80.02 |
| 275 | 3.64 | 69.05 | 73.50 | -168.05 | -165.67 | -145.26 | -82.15 |
| 298.15 | 3.35 | 65.16 | 68.78 | -170.50 | -168.33 | -146.19 | -83.98 |
| 400 | 2.5 | 53.48 | 54.66 | -181.77 | -181.11 | -149.83 | -90.79 |
| 600 | 1.67 | 42.32 | 41.24 | -205.72 | -210.17 | -155.34 | -100.44 |
| 700 | 1.43 | 39.21 | 37.52 | -218.37 | -226.22 | -157.54 | -104.16 |
| 800 | 1.25 | 36.91 | 34.79 | -231.38 | -243.10 | -159.49 | -107.41 |
| 900 | 1.11 | 35.15 | 32.70 | -244.70 | -260.69 | -161.24 | -110.27 |
| 1000 | 1.00 | 33.77 | 31.07 | -258.31 | -278.93 | -162.82 | -112.85 |
| 1100 | 0.91 | 32.65 | 29.76 | -272.16 | -297.74 | -164.26 | -115.18 |
| 1200 | 0.83 | 31.74 | 28.69 | -286.24 | -317.08 | -165.59 | -117.32 |
| 1300 | 0.77 | 30.98 | 27.81 | -300.52 | -336.91 | -166.82 | -119.28 |
| 1400 | 0.71 | 30.34 | 27.06 | -315.00 | -357.17 | -167.97 | -121.11 |

## HOMO and LUMO energy analysis of mercury-containing species on 5×5×2 CaO clusters

HOMO (the highest occupied molecular orbital) and LUMO (the lowest unoccupied molecular orbital) energy levels, and band gaps for the Hg, HgCl and $HgCl_2$ on clean 5×5×2 CaO clusters were calculated with the GGA/BLYP functional. The HOMO, LUMO energy levels and HOMO&LUMO energy gaps are shown in Fig. 6. HOMO – LUMO energy gaps are important in explaining the stabilities of the adsorption models. The clean CaO cluster had π* molecular orbitals which are formed from 4 s(Ca) and 2p(O) atomic orbitals in a diagonal direction while the middle oxygen atom had the highest energy state due to relaxation effects. The HOMO and LUMO energy level decreases as the mercury is oxidized. The HOMO energy level of HgCl on the 5×5 CaO surfaces significantly dropped. The largest band gap occurred for HgCl adsorption and the HOMO for HgCl adsorption was localized between the adsorbate and the middle of the surface through strong interactions with the first layer. There was a degenerate set of occupied π* molecular orbitals between the σ and σ* orbitals for the HOMO of the HgCl molecule. Occupied π* molecular orbitals occurred with the destabilization of the HgCl bond and inhibited the stabilization of the π bonding electrons. This lone pair destabilizing effect generated an HgCl molecule that was strongly bonded to the CaO cluster models. The results of large energy gaps for HgCl and $HgCl_2$ on the CaO surface show high stabilities which allow calcium oxide to remove oxidized mercury effectively. When the chlorine atoms were adsorbed on top of the calcium atoms of the surface, the LUMO energy levels dropped. The relaxation on the surface influenced oxidized mercury species adsorption by also significantly lowering HOMO energy levels. These results indicate that the $HgCl_2$ adsorbate had strong interactions with the relaxed CaO surface, as much as HgCl adsorption, leading to similar adsorption energies.

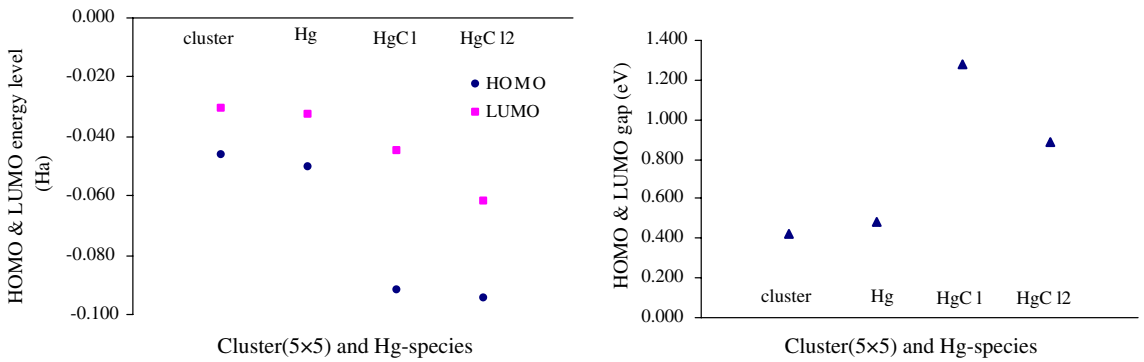


**Fig. 6** The plots of HOMO and LUMO energy levels and the HOMO & LUMO energy gap for Hg, HgCl and $HgCl_2$ adsorption on 5×5 CaO cluster models with GGA/BLYP functionals (HOMO and LUMO energy levels are in Hartree, and band gaps are in eV)

## Conclusions

DFT calculations were used to investigate the adsorption of mercury-species on relaxed CaO surfaces with LDA/PWC calculations for the geometry optimization and GGA/BLYP functionals for the adsorption energies. On the 5×5×2 CaO cluster and periodic slabs, optimized geometries and adsorption energies had similar trends. The mercury adsorbed on an atop site of the middle oxygen while chlorine bonded with a calcium site. Mercury has a shorter distance to oxygen as mercury is oxidized for the 5×5×2 cluster and periodic models. The chlorine atom contributes to the shorter Hg – O bond although Cl moves further from the surface. The calculated adsorption energies of $HgCl_2$ adsorption on relaxed 5×5×2 cluster and periodic slab models were stronger by -70.96 ~-97.65 kJ $mol^{-1}$ than on the fixed CaO models, placing them in the chemisorption range rather than being at the threshold between physisorption and chemisorption. This was due to the relaxation effects. However, adsorption energies of Hg and HgCl adsorption were not changed compared to the fixed surface. Adsorption energies of Hg on a 5×5×2 cluster and periodic slab were placed in the physisorption range. The number of surface layers does not strongly affect adsorption geometry or energy for $HgCl_2$ adsorption on periodic slab systems after comparison between adsorption results on 5×5×2 and 5×5×3 periodic slab systems. Moreover, thermodynamic data of oxidized mercury adsorption on the CaO surface at all temperature ranges are not significantly dependent on the number of surface layers. This proves that two layer surfaces are sufficient for mercury-containing species adsorption on metal oxide surface. Finally, the CaO component of MinPlus sorbents could be a strong adsorbent to capture oxidized mercury, $HgCl_2$.

**Acknowledgments** This research was supported by the Department of Energy, Grant # DE-FC26-04NT42313.

## References

1. Pirrone N, Cinnirella S, Feng X, Finkelman RB, Leaner J, Mason R, Mukherjee AB, Stracher GB, Streets DG, Telmer K (2010) Atmos Chem Phys Discuss 10:4719–4752
2. Scala F (2001) Environ Sci Technol 35:4373–4378
3. Scala F (2001) Environ Sci Technol 35:4367–4372
4. Otani Y, Emi H, Kanaoka C, Uchijima I, Nishino H (1988) Environ Sci Technol 22:708–711
5. Otani Y, Kanaoka C, Usui C, Matsui S, Emi H (1986) Environ Sci Technol 20:735–738
6. Olsen ES, Laumb JD, Benson SA, Dunham GE, Sharma RK, Mibeck BA, Miller SJ, Holmes MH, Pavlish JH (2003) J Phys IV 107:979–982
7. Lancia A, Karatza D, Musmarra D, Pepe F (1996) J Chem Eng Jpn 29:939–346
8. Krishnan SV, Gullett BK, Jozewicz W (1994) Environ Sci Technol 28:1506–1512
9. Karatza D, Lancia A, Musmarra D, Pepe F, Volpicelli G (1996) Hazard Waste Hazard Mater 13:95–105
10. Jurng J, Lee TG, Lee GW, Lee SJ, Kim BH, Seier J (2002) Chemosphere 47:907–913
11. Hocquel M, Unterberger S, Hein KRG (2001) Chem Eng Technol 24:1267–1272
12. Ghorishi SB, Singer CF, Jozewicz WS, Sedman CB, Srivastava RK (2002) J Air Waste Manage Assoc 52:273–278
13. Chang JCS, Ghorishi SB (2003) Environ Sci Technol 37:5763–5766
14. Changsuphan A, Kerdsuwan S, Bashkin VN (2003) J KMITNB 13:2546–2553
15. EPA-452/R-97-010 An Evaluation of Mercury Control Technologies and Cost (1997) Mercury study report to congress Vol. 8:ES-11–ES-14
16. Luo Z, Hu C, Zhou J, Cen K (2006) Fuel Process Technol 87:679–685
17. Wendt JOL, Lee SJ, Biermann J (2007) 6th International Symposium on Coal Combustion (ISCC). China Dec, Wuha, pp 1–4
18. Zeng H, Jin F, Guo J (2004) Fuel 83:143–146
19. Sliger RN, Kramlich JC, Marinov NM (2000) Fuel Process Technol 65:423–438
20. Galbreath KC, Zygarlicke CJ (1996) Environ Sci Technol 30:2421–2426
21. Kim BG, Li X, Blowers P (2009) Langmuir 25:2781–2789
22. Trubitsyn DA, Zakharov VA, Zakharov II (2007) J Mol Catal A Chem 270:164–170
23. Karlsen EJ, Nygren MA, Pettersson LGM (2002) J Phys Chem A 106:7868–7875
24. Pacchioni G (2000) Surf Rev Lett 7:277
25. Noguera C (2001) Surf Rev Lett 8:121
26. Freund HJ, Kuhlenbeck H, Staemmler V (1996) Rep Prog Phys 59:283–347
27. Broqvist P, Gronbeck H, Panas I (2004) Surf Sci 554:262–271
28. Delley B (1990) J Chem Phys 92:508–517
29. Materials Studio, Accelrys, Inc.: San Diego, CA (2001)
30. Perdew JP, Wang Y (1992) Phys Rev B 45:13244–13249
31. Jaffe JE, Hess AC (1996) J Chem Phys 105:10983–10998
32. Perdew JP, Burke K, Ernzerhof M (1996) Phys Rev Lett 77:3865–3868
33. Pacchioni G (2002) Surf Sci 520:3–5
34. Mattsson AE, Jennison DR (2002) Surf Sci 520:L611–L618
35. Kantorovich LN, Gillan MJ (1997) Surf Sci 374:373–386
36. De Leeuw LH, Purton JA, Parker SC, Watson GW, Kresse G (2000) Surf Sci 452:9–19
37. Curtiss LA, Raghavachari K, Trucks GW, Pople JA (1991) J Chem Phys 94:7221–7230
38. Lee C, Yang W, Parr RG (1988) Phys Rev B 37:785–789
39. Becke AD (1998) Phys Rev A 38:3098–3100
40. Becke AD (1988) J Chem Phys 88:2547–2553
41. Chase MW Jr (1998) NIST-JANAF themochemical tables, 4th edn. J Phys Chem Ref Data Monograph 9:1–1951
42. Zhang N, Blowers P, Farrell J (2005) Environ Sci Technol 39:4816–4822
43. Xu YJ, Zhang YF, Lu NX, Li JQ (2004) Phys Rev B Condens Matter 348:190–197
44. Jensen MB, Pettersson LGM, Swang O, Olsbye U (2005) J Phys Chem B 109:16774–16781
45. Williams SD, Edwards EE (2004) Int J Mol Sci 5:67–74
46. Huda MN, Ray AK (2005) Int J Quantum Chem 102:98–105
47. Cremer D, Kraka E, Filatov M (2008) Chem Phys Chem 9:2510–2521
48. Simperler A, Watt SW, Bonnet PA, Jones W, Motherwell WDS (2006) Cryst Eng Commun 8:589–600
49. Adamson AW, Gast AP (1997) Physical chemistry of surfaces, 6th edn. Wiley, New York
50. Loffreda D (2006) Surf Sci 600:2103–2112